

Delft University of Technology  
Master's Thesis in Embedded Systems

# Transiently-powered Battery-free Robot

Koen Schaper





# Transiently-powered Battery-free Robot

Master's Thesis in Embedded Systems

Embedded Software Section  
Faculty of Electrical Engineering, Mathematics and Computer Science  
Delft University of Technology  
Mekelweg 4, 2628 CD Delft, The Netherlands

Koen Schaper  
kpschaper@gmail.com

11th December 2017

**Author**

Koen Schaper (kpschaper@gmail.com)

**Title**

Transiently-powered Battery-free Robot

**MSc presentation**

15 December 2017

**Graduation Committee**

prof. dr. K.G. Langendoen (chair)

Delft University of Technology

dr. Przemysław Pawełczak (supervisor)

Delft University of Technology

dr. Javier Alonso-Mora

Delft University of Technology

## **Abstract**

Collectives of miniature robots are envisioned to have future applications in surveillance, search and rescue operations, and exploration. However, before these robots can become applicable in real-world applications, a fundamental challenge related to supply of energy needs to be addressed first. That is, the operation time of small robots is currently limited by the energy storage in batteries. Unfortunately, new advancements in batteries are not expected to happen anytime soon, the history shows that new battery technologies are slow emerging. Therefore, this thesis proposes to replace the battery with an energy harvester and temporarily store harvested energy in a supercapacitor. This results in a new phenomenon to be taken into consideration in designing a robot: frequent power failures due to the intermittent availability of energy. Intermittency is currently not taken into account in the development process of a robot, and its effect on control techniques and accuracy of movement is, therefore, unexplored. In this thesis a transiently-powered battery-free robot is developed that purely operates on harvested energy from light. The robot is able to move with a 16% power duty cycle, using a lighting setup consisting of four halogen lamps. With the help of local feedback the robot is able to perform controlled movements, while variables stored in non-volatile memory enable the robot to save the movement progress across power cycles. The movement accuracy of the transiently-powered robot is evaluated using tracking software to extract the exact path of movement from straight and circular motion recordings. The transiently-powered robot shows minimal increased deviation from its instructed path when compared to its battery powered equivalent, given an experimentally determined minimum on time of 0.3 s. The results prove the feasibility of a transiently-powered battery-free robot, clearing a potential path for self-sufficient and energy-autonomous small robots.



# Preface

This thesis presents the final step towards obtaining my Master's degree in Embedded Systems from Delft University of Technology. To the best of my knowledge no previous work has been conducted, exploring the feasibility of a transiently-powered battery-free robot.

I would like to express my sincere gratitude to my supervisor Przemysław Pawełczak for his excellent guidance, never failing support and enthusiasm about this project. I also would like to thank Amjad Majid for letting me explore his idea of transiently-powered actuation, his constructive criticism and clever suggestions as this project evolved. Moreover, I would like to thank Sinan Yıldırım for his willingness to answer any of my questions, Ioannis Protonotarios for helping me with any hardware related issues and Michel Jansen for sharing his energy harvester schematics (given in Appendix A). Additionally, I would like to thank the Nuon Solar Team for lending me one of their space grade solar panels from their 2017 Nuna9 solar car. Furthermore, I want to thank Prof. Koen Langendoen for hosting me at the Embedded Systems group, and Javier Alonso-Mora for participating as a member of my graduation committee. Last but not least, a special thanks to my family for their unconditional support, encouragements and love that helped me stay motivated during this year.

Koen Schaper

Delft, The Netherlands  
11th December 2017



# Contents

<b>Preface</b>	<b>v</b>
<b>1 Introduction</b>	<b>1</b>
1.1 Problem statement . . . . .	2
1.2 Contributions . . . . .	2
1.3 Thesis Outline . . . . .	3
<b>2 Related Work</b>	<b>5</b>
2.1 Transiently-powered Systems . . . . .	5
2.2 Computation across Power Cycles . . . . .	6
2.3 Energy Storage . . . . .	6
2.4 Small Robotic Platforms . . . . .	6
2.5 Locomotion . . . . .	7
2.6 Continuous Operation . . . . .	8
<b>3 Preliminaries</b>	<b>11</b>
3.1 Design requirements . . . . .	11
3.2 Energy Source Selection . . . . .	12
3.2.1 Energy Harvesting and Storage . . . . .	12
3.2.2 Measuring the Charge Time . . . . .	12
3.2.3 Energy Harvesting from radio signals . . . . .	12
3.2.4 Energy Harvesting from Light . . . . .	13
3.2.5 Conclusion . . . . .	14
3.2.6 Light setup . . . . .	15
3.3 Locomotion Selection . . . . .	15
3.3.1 Stepper motor-based Locomotion . . . . .	16
3.3.2 DC Motor locomotion . . . . .	18
3.3.3 Conclusion . . . . .	19
<b>4 Design and Implementation</b>	<b>21</b>
4.1 Hardware Design . . . . .	21
4.1.1 Energy Harvesting and Storage . . . . .	22
4.1.2 Computation . . . . .	22
4.1.3 Sensing . . . . .	22

4.1.4	Locomotion . . . . .	23
4.1.5	Motor Control . . . . .	23
4.1.6	Integration . . . . .	23
4.1.7	Energy Expenditure . . . . .	23
4.1.8	Costs . . . . .	24
4.2	Motion Control Design . . . . .	25
4.2.1	PWM Frequency for Linear Motion Control . . . . .	25
4.2.2	Closed loop feedback for controlled movements . . . . .	27
4.3	Software Implementation . . . . .	28
4.3.1	Control loop . . . . .	29
4.3.2	Motor Control . . . . .	30
4.3.3	Persistent Movement . . . . .	31
4.3.4	Extendability . . . . .	31
<b>5</b>	<b>Evaluation</b>	<b>33</b>
5.1	Controlled Movements . . . . .	33
5.1.1	Experimental setup . . . . .	33
5.1.2	Straight Movements . . . . .	36
5.1.3	Circular Movements . . . . .	38
<b>6</b>	<b>Summary</b>	<b>41</b>
6.1	Conclusion . . . . .	41
6.2	Future Work . . . . .	42
<b>A</b>	<b>Schematic of the Robot PCB</b>	<b>49</b>

# Chapter 1

## Introduction

Miniature robots with limited capabilities in locomotion and sensing, can work together as a collective to achieve more than an individual could by itself. The future potential of collectives of small robots, i.e. swarms, is widely recognized to have applications in surveillance, search and rescue operations, and exploration. Swarms have also been proposed as a new form of user interface. For instance, small robots can interact with users on tabletops [1], unmodified clothing [2] and can be an educational toy for kids [3], as seen in Figure 1.1.

However, advanced swarms are still far from being applicable in real-world applications [4]. One of the fundamental issues that needs to be addressed is related to the supply of energy. Small lithium batteries are currently powering the robots and limit their operation time to only a few hours. To give a stark example, the energy density of batteries has improved less than one order of magnitude since 1945, while in comparison the energy efficiency of computing has improved 12 orders of magnitude [5]. The last major advancement in battery technology is 25 years old and came with the introduction of Li-ion batteries. Additionally, any new big improvements in energy density of batteries is not likely to happen anytime soon, as new battery technologies are often overhyped and slow to emerge [6].

Stable energy supplies are considered a requirement to allow long term persistent operation of robots. As of now, different replenishment methods for robot batteries are currently used, robots can be moved to a charging station, which leaves them non-operational. At the same time, manual recharging or battery replacement results in a high strain on maintenance. Therefore, relaxing the stable energy supply constraint by allowing a transient supply of harvested energy could be a potent area of research.



(a) Zooids [1]

(b) Rovables [2]

(c) Sony Toio [3]

Figure 1.1: Current applications for small robotic platforms, ranging from swarm user interfaces and mobile wearables to educational toys for kids.

## 1.1 Problem statement

Replacing a battery with an energy harvesting system could make a robot self-sufficient and energy-autonomous. However, this introduces a new phenomenon that has to be taken into account: the *intermittent availability* of energy produces frequent power interrupts. The possibility of sudden power loss is currently not considered when developing control software for a robot, and for this reason can not be used without applying methods to preserve computation across power cycles.

Furthermore, applicable sensors and/or sensing frequency may be constrained due to the limited energy budget. The largest part of the energy budget is likely to be already consumed by the actuators that supply movement to the robot. Not every actuator currently used for movement may be reliable and/or accurate under the frequent power interruption. Therefore, the research question this work addresses is:

*What is the effect of intermittency on the movement accuracy of a transiently-powered robot without external feedback?*

## 1.2 Contributions

The software controlling robots currently assumes that a task can only be completed if sufficient energy is left in the batteries, which inherently limits their operation time. This research explores the feasibility of a miniature battery-free robot, allowing persistent operation while being supplied by a small and intermittent source of energy. The list of contributions is as follows:

1. The design of a battery-free robot that purely operates from harvested energy, with basic capabilities allowing autonomous operation.

2. The implementation of local movement feedback, that allows the robot to finish a movement across power cycles.

### 1.3 Thesis Outline

The rest of the thesis is organized as follows: Chapter 2 provides background information and introduces the related work. The preliminaries in design of the transiently-powered robot are presented in Chapter 3. In Chapter 4 the hardware design and software implementation are explained. This is followed by a performance evaluation of the transiently-powered robot in Chapter 5. Finally, Chapter 6 concludes this thesis and proposes potential future work.



## Chapter 2

# Related Work

Background information about state-of-the-art transiently-powered systems is provided in Section 2.1. In Section 2.2 methods that allow computation across power cycles are discussed. The advantages and disadvantages of different electrical storage types are compared in Section 2.3. A short summary of current miniature robotics platforms is given in Section 2.4 and commonly used locomotion types are discussed in Section 2.5. Finally, different methods that try to ensure continuous operation are discussed in Section 2.6.

### 2.1 Transiently-powered Systems

Transiently-powered systems have evolved from the need to remove batteries, and instead harvest energy from ambient sources. The ambient sources available for exploration are determined by the environment, and can be scarce or completely absent during prolonged time intervals of the day [7]. As a result, the amount of power harvested can vary significantly over time, and an energy buffer is required to guarantee the ability to complete a task.

Fully programmable RFID platforms have been developed that explore the combination of sensing, computation and communication, while allowing battery-less operation [8]. These platforms are powered from the radio signal emitted by a specialized RFID reader. The harvested energy is stored in a capacitor, larger capacitors can buffer more energy while smaller capacitors have the advantage of shorter charge times [9]. For longer operations that cannot be interrupted, the energy budget needs to be evaluated carefully. To store the energy, an appropriate size storage capacitor needs to be selected, since increasing the size also increases the self discharge rate of the capacitor [10]. The buffer still limits the operation time, resulting in frequent system power failures.

## 2.2 Computation across Power Cycles

To be able to execute long running-programs under the threat of power loss due to the energy buffer depletion, different methods have been developed to allow computation across power cycles. There are several methods that propose solutions to computation across power cycles. For example, programs can be automatically transformed to run under frequent loss of power by using energy-aware state checkpointing. The state of the program is saved in non-volatile memory before running out of energy [11]. Another checkpointing method removes the need for special hardware or a programming model, instead it uses a compiler to add lightweight non-volatile checkpoints to a program, dividing it into re-executable sections [12]. Besides that, other research proposes a new programming model that splits a program into tasks, where the tasks exchange data through non-volatile input and output channels, guaranteeing consistency of the program [13].

## 2.3 Energy Storage

Internet of Things (IoT) devices are currently powered from one of two sources, either from batteries or supercapacitors. Normal capacitors cannot store enough energy to power devices and are mainly used to stabilize power supplies. Each electrical storage technology has different properties, as seen in Table 2.1. For example, supercapacitors have a higher power density that allows for quick charge and discharge rates without any special charging circuitry [14]. Supercapacitors are more safe when used outside their recommended operating conditions, as they do not contain any toxic chemicals like batteries [15]. The two largest disadvantages of super-capacitors are their low energy density and high price.

On the other hand, batteries have a higher energy density when compared to supercapacitors and in addition, experience lower leakage currents. A downside of using batteries is that they seldom withstand more than one thousand complete charge/discharge cycles. Overheating of batteries can severely reduce the lifetime of a battery or in the worst case lead to explosion, which happened to the Galaxy Note 7 from Samsung in January [16].

## 2.4 Small Robotic Platforms

Reducing the size of robots has a number of benefits. First of all, the amount of materials to build a single robot is reduced, which often lowers the final production cost. Low cost robots are, for example, developed to make them available for educational use and allow children to come in contact with robotics and programming at an early age [18].

Table 2.1: Characteristics comparison of capacitors, supercapacitors and batteries [17]. Capacitors can store less energy than batteries, but have a higher power density and a larger cycle life.

Characteristics	Capacitor	Supercapacitor	Li-ion battery
Specific Energy (Wh/kg)	<0.1	1–10	10–100
Specific Power (W/kg)	>10.000	500–10.000	<1000
Discharge time	$10^{-5}$ to $10^{-3}$ s	s to min	0.3–3 h
Charge time	$10^{-5}$ to $10^{-3}$ s	s to min	1–5 h
Coulombic efficiency (%)	About 100	85–98	70–85
Cycle life	Almost infinite	>500.000	about 1000

Cost and size can also be a main design considerations when developing miniature robots to research swarm behavior. Keeping the cost down allows experiments with larger collectives of swarm robots that work together to achieve a single goal. Hardware modularity is exploited to make robots adapt their resources to different environments and sensing operations. By separating power, computation, motor control and sensing, a variety of capabilities can be tested [19, 20, 21].

In order to remotely operate and/or coordinate a collective, the robots require communication with a global host accomplished by means of active low power transceivers [19, 20, 21]. Other microrobots use infrared-based communication, which is additionally used for neighbor to neighbor distance sensing [22]. Batteries power these small robots and provide roughly one to three hours of energy. An overview of current state-of-the-art small robotic platforms is provided in Table 2.2.

## 2.5 Locomotion

Choosing the method of actuation that allows the robot to move, i.e. locomotion type, can depend on different factors. Moving in the most energy efficient way on a particular surface is often the determining factor. On a flat surface, robots commonly use a two-wheeled differential drive design to not only move but allow for steering as well [19, 20]. The need for wheels can be eliminated by positioning the DC motors at a 45 degree angle relative to surface and letting the motor shafts directly contact the surface [21]. A tiny ball caster is used as a third support point in the front of the robot. Other designs do not use conventional DC motors, but instead use stepper motors. The motors speed can be set by changing the delay between steps. Estimating position is therefore reduced to simply counting steps [20].

Another decisive factor can be the overall cost. Vibrating motors can be combined with three thin legs [22]. When the vibrating motors are activated the centripetal forces generate a forward movement, which can be explained using the slip-stick principle. Other locomotion types are biologically in-

spired, a small scale piezoelectric driven quadruped robot is designed to decrease manufacturing complexity and overall cost [23].

## 2.6 Continuous Operation

Typically, the operation time is extended by regularly checking the remaining energy in the battery and move to a recharging station before the robot runs out of energy [20, 22].

An alternative to quick recharging is to swap the battery automatically when the robot moves into the docking station [24]. An example is a robot which is able to swap its primary battery using a six degree-of-freedom manipulator. The manipulator is used to grab the dead battery and plug it into a wireless recharging charging station [25].

Direct wireless power can be used as an alternative to batteries to provide power to a robot [26]. However, the robot can only operate or recharge while it remains in proximity to a transmitter. In this case the robot is highly reliant on an infrastructure to allow for continuous autonomous operation, and can not operate in an area where this infrastructure is not present.

Persistent operation can be achieved by harvesting renewable energy to complement to the robots internal energy source. To remove weight from the robot, in [27] the solar energy is used directly without any type of energy buffer. A drawback of this method is that the incoming solar energy should be greater or equal to the energy required for operation. This approach has only been tested for basic locomotion and has not combined any form of sensing or control.

Table 2.2: The small robotic platforms are compared in cost, size and weight. It is clear that the transiently-powered robot has tiny energy capacity, very short operation time but the ability to recharge locally.

Robot	Cost (€)	Locomotion	Speed (cm/s)	Size (mm <sup>†</sup> )	Weight (g)	Energy Capacity (mAh)	Operation Time	Recharge Method
This robot	59	wheel	25	35×40	22	0.006	1 s	solar
Roverables [2]	34 <sup>‡</sup>	wheel	N/A	40×26	36 <sup>‡</sup>	100	45 min	inductive
Zoids [1]	43	wheel	50	26×26	12	100	1 h	manual
mROBERTO [21]	52 <sup>‡</sup>	motor shaft	15	16×16	10 <sup>‡</sup>	120	1.5 h	manual
GRITSBot [20]	43 <sup>‡</sup>	wheel	25	31×30	60 <sup>‡</sup>	150	1 h	contact
TinyTerp [19]	43	wheel	50	17×18	N/A	50	1 h	manual
Kilobot [22]	43 <sup>‡</sup>	vibration	1	33×33	17.6 <sup>‡</sup>	160	3 h	manual (bulk)
HAMR-VP* [27]	N/A	legged	44	44×44	2.3	8	3 min	manual

\* Modified to include on-board power, sensing and control.

<sup>†</sup> Cost of parts

<sup>‡</sup> Obtained by contacting the authors of the paper



# Chapter 3

## Preliminaries

The design requirements for the robot is explained based on minimal required capabilities in Section 3.1. Section 3.2 evaluates two sources for energy harvesting and in Section 3.3 two types of locomotion for the transiently powered robot are evaluated.

### 3.1 Design requirements

This section explains the main areas considered while designing the battery-less transiently-powered robot.

1. **Power:** The robot should not rely on batteries. Energy can be harvested from ambient sources and stored in a supercapacitor. Energy harvested in a controlled environment should charge the capacitor in under 10 seconds and stored energy should provide at least an operation time of 1 second i.e. a minimal 10% power duty cycle.
2. **Small form factor:** The size and weight of the robot needs to be kept to a minimum, reducing the energy required for movement. Additionally, designing the robot to use low cost off-the-shelf parts makes it convenient to build collectives of small transiently-powered robots.
3. **Locomotion:** An efficient locomotion type needs to be selected for the movement on flat surfaces, to optimize the distance that can be covered with a single capacitor charge.
4. **Controlled movements:** Despite the frequent power failures, the transiently-powered robot needs to be able to complete a movement with an acceptable error when compared to its battery powered counterpart.

## 3.2 Energy Source Selection

In this section two sources for the harvesting of ambient energy are evaluated: radio signals and solar. The charge times of an energy storage element are measured for a variety of distances from the selected sources.

### 3.2.1 Energy Harvesting and Storage

Energy is harvested using a Texas Instruments BQ25570 energy harvester [28], which includes a nanopower boost charger with maximum power point tracking to extract the optimal amount of energy. The harvested energy is stored in a 22 mF - 4.5 V supercapacitor from AVX [29], chosen for its low leakage current and small size. The BQ25570 comes with a buck converter to efficiently regulate the capacitors voltage down to the system voltage of 2.2 V. External resistors are used to program voltage thresholds, allowing to automatically enable and disable the buck converter based on minimum and maximum thresholds. The minimum threshold is set to 2.2 V and the maximum threshold is set to 4.2 V.

### 3.2.2 Measuring the Charge Time

The buck converter of the energy harvester is automatically enabled when the maximum voltage threshold is reached. A load is connected to the output of the buck converter to quickly drain the energy from the capacitor. In this case load is chosen such that the power consumed by the load  $P_{\text{load}} \gg P_{\text{in}}$ , the harvested input power . By connecting a Saleae logic analyzer [30] to the output of the buck converter, the off time of the power cycles can be recorded. The time that the output of the buck converter is disabled is equal to the time to charge the capacitor from the minimum to the maximum threshold.

### 3.2.3 Energy Harvesting from radio signals

#### Harvesting using a WISP

To be able to connect an external harvester, a WISP 5 [8] is modified. The integrated energy harvester, the storage capacitor and the diode to bypass the harvester, are removed from the WISP. A wire is soldered to the input pin pad of the removed harvester on the WISP PCB. This wire is connected directly to the input of the external energy harvester.

#### Measurements

Energy is provided to the WISP using a Impinj Speedway R1000 RFID reader [31, 32]. This reader is connected to a Laird S90028PCR antenna [33].

Table 3.1: The average charge time by harvesting energy from RFID transmitter.

Distance from RFID reader (cm)	25	35	45
Average charge time (s)	49.1	61.1	164.8

Table 3.2: Specification of the three solar panels tested in the experiment.

	Material	Efficiency (%)	Dimensions (mm)
Banggood [34]	Poly-Si	17	40x30
INYS SLMD121H04L-ND [35] <sup>1</sup>	Mono-Si	22	43x34
AzurSpace 3G28C [36]	Triple Junction GaAs	28	80x40

<sup>1</sup> Two panels in parallel

The WISP is positioned 25, 35 and 45 cm away from the reader and the charge times are recorded.

## Results

The time to charge the capacitor is more than 49 s, see Table 3.1. As the WISP is placed further away from the reader the charge times increase significantly. While the distance increases the harvested power is decreased due to path loss and reflections of the signal.

### 3.2.4 Energy Harvesting from Light

Sunlight is not always available or strong enough to charge the robots supercapacitor in acceptable time. Alternatively, lamps can provide uniform light to the area where the robot moves around. In this section the capacitor charge time is evaluated for different solar panel and light source combinations. To accurately measure the power that is harvested from each solar panel, their performance was evaluated in a darkroom at TU Delft Embedded Software Lab.

#### Solar panels

Three solar panels are tested, each different in material, efficiency and panel size, as seen from Table 3.2.

#### Lamps

Low cost solar simulators can for example consist of a combination of LED and halogen light bulbs to simulate sunlight and are used to test the performance of solar panels [37]. However, the goal is to have a controlled uniform lighting environment where the robots have roughly constant charge times. Solar panels do not only harvest energy from the visual light spectrum but

harvest at least as much from the infrared light spectrum, therefore not only light but also heat shortens the charge time [35]. Halogen lamps have a lower color temperature than the sun, but also emit waves far into the infrared spectrum. The light sources used in this experiment are a 60 W halogen bulb, a 120 W halogen bulb and two 150 W Philips BR125, infrared (IR) incandescent reflector lamps [38] where one is translucent and the other uses a red filter.

## Measurements

Three charge time measurements are performed, each lamp is positioned 10 cm, 30 cm and 50 cm from the solar panels. As reference, the charge times are also measured on a sunny November afternoon, inside the office room of TU Delft Embedded Software lab.

## Results

The results obtained from the measurements show a non-linear relation between the charge times and the distance between the solar panel and the source, as seen in Table 3.3. Increasing the output power of the source and decreasing the distance between panel and the source, both decrease the charge times. However, there is no obvious best performing combination of solar panel/light source.

Note that with some lamps a shadowing pattern is observed due to the construction of the lamps. The 60 W and 150 W IR lamps have a spherical design, and their construction creates an uneven circular shadowing pattern. This becomes more significant on larger distances. The 120 W halogen lamp has a tubular design and in combination with the light fixture most of the light is reflected down with minimal shadowing of the lamp resulting in a more even light distribution. Therefore, it is chosen to provide light in the controlled setup where the robots can move around with roughly constant charge times. For the 120 W halogen lamp at the distances 30 cm and 50 cm the INYS solar panel seems to perform the best.

Additionally, the charge times were recorded during a sunny 30 minute time slot (2:30–3:00 PM, 23 November 2017) for each solar panels, as seen in Table 3.4. The Azurspace solar panel has the shortest supercapacitor charge time, this can be expected because the triple junction allows it to harvest energy from the broadest part of the light spectrum.

### 3.2.5 Conclusion

The results from RF experiments show that the minimum charge time is 49 s, which more than doubles with only a 20 cm distance increase from the reader. Light is more readily available and by illuminating the area where the robot moves around with a 120 W halogen lamp source, 6 s charge times

Table 3.3: The average supercapacitor charge times, for each panel at three distances from the sources.

Distance (cm)	Panel	Average charge time per source (s)			
		60 W	120 W	150 W clear	150 W red
10	Banggood	3.08	2.19	0.99	0.73
	INYS	2.52	0.75	0.46	0.51
	Azurspace	5.62	3.22	1.55	3.54
30	Banggood	6.45	6.72	7.83	1.88
	INYS	8.00	5.68	2.67	1.50
	Azurspace	23.05	8.25	19.75	20.33
50	Banggood	26.28	17.59	17.91	9.46
	INYS	45.41	15.53	9.28	6.97
	Azurspace	106.67	24.18	46.20	93.91

The charge times are normalized to a panel dimension of 40×40 mm.

Table 3.4: The average charge time harvesting ambient light during a sunny afternoon.

Panel	Charge time (s)
Banggood	3.84
INYS	3.55
Azurspace	2.81

can be achieved when the light is positioned at a distance of 30 cm from the solar panel. With the solar panel eight times shorter charge times can be achieved, and therefore solar is chosen to be the energy source for the transiently-powered robot.

### 3.2.6 Light setup

To create an area where the transiently-powered robots can move around with approximately constant charge times, a light setup is created using wooden beams, as shown in Figure 3.1. Mounted in this frame are four 120 W halogen lamps, previously determined to provide the most uniform light distribution and short charge times. The frame spans an area of 95×66 cm and distances the lamps 30 cm from the tabletop.

## 3.3 Locomotion Selection

Wheeled locomotion types are assumed to be the most efficient on flat surfaces. Therefore, in this section two wheeled locomotion types are evaluated: the stepper motor and the DC motor. The robot can navigate without ex-

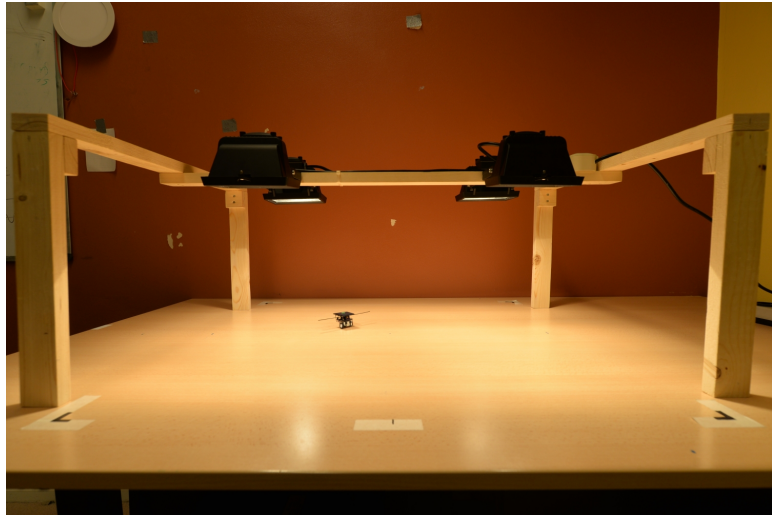


Figure 3.1: The light setup consisting out of four halogen lamps placed 30 cm from the table top, providing energy to the robot.

ternal feedback from one location to another, but accurate locomotion and basic odometry are required.

### 3.3.1 Stepper motor-based Locomotion

The GRITSBot [20] uses stepper motor based locomotion which already include basic odometry, as described in Section 2.5. The upcoming section further investigates the use of stepper motor based locomotion for a transiently-powered robot.

#### Operation of a Stepper Motor

Stepper motors are permanent magnet DC motors that start to rotate by supplying current to the motor coils in a specific direction. The bipolar stepper motor used, requires current to be pulsed through each of the four connections, in a fixed pattern, in order to rotate it forwards or backwards. A Microcontroller (MCU) is used to keep track and control stepper motor position from a sequence of four. The outputs of the MCU cannot supply enough current to drive a bipolar stepper motor, therefore a dual H-bridge is required to control the current through each coil.

#### Control and Rotor Synchronization

The only way to guarantee that the rotor stays aligned with the coil, is to keep the coil energized until the next position is instructed and the succeeding coil is energized. On the first startup the rotor may not be aligned with

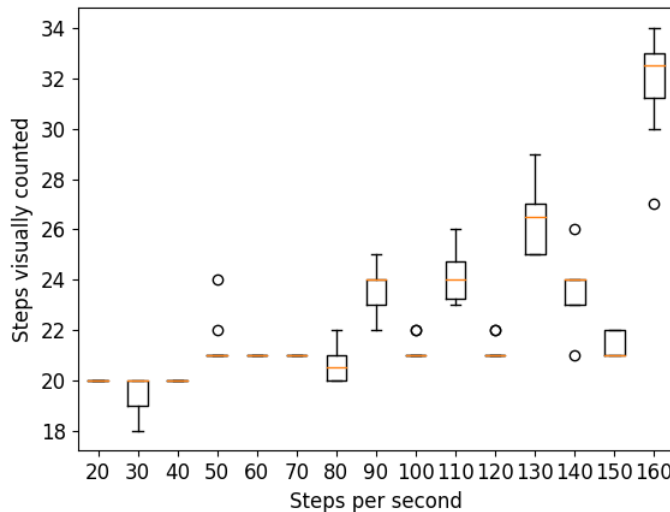


Figure 3.2: The visually counted number of steps when power is removed after 20 steps. The stepper motor is likely to overshoot and this effect becomes more significant with increased step frequency.

the last position in the sequence of four. As a result an error between one and three steps can occur before the energized coil and rotor are synchronized.

In case the stepper motor is rotating and the power is removed, misalignment between the rotor and the last energized coil can occur. While the rotor could be moving from one position to the next, it has not moved at all (undershoot) or can continue to move to the next position due to inertia of the rotating mass (overshoot). To determine what would be more likely, undershooting or overshooting, the following experiment has been performed to determine the error in the number of steps.

### Experimental setup

The motor used for this experiment is a 6 mm permanent magnet bipolar stepper motor from Nidec [39]. For this motor one rotation is equal to 20 steps i.e. five times the sequence of four. This stepper motor is suspended and a needle glued to the motor shaft. The needle rotates over a round piece of paper which is divided by markings in 20 steps. First the rotor and coil are synchronized by moving four steps, and the position of the needle is visually recorded and written down. Then the stepper motor is commanded to make one rotation equal to 20 steps. After rotating 20 steps the power is removed from the coils and the needle position is again visually recorded and written down.

## Stepper Motor Inertia Result

Figure 3.2 shows the result of the experiment. The stepper motor on average overshoots, i.e. does more steps than commanded when the power is removed. This effect becomes more significant with increased step frequency. While this experiment only shows the effect for an unloaded motor, it is likely that a synchronization error also occurs when a transiently-powered robot would be powered using two stepper motors in differential drive. After every power interrupt, the rotor of each motor needs to be synchronized with the energized coil by the MCU. As a result the robot could make a random turn if the error between the motors is not equal.

### 3.3.2 DC Motor locomotion

Small DC motors are commonly selected to provide locomotion for small robotic platforms as seen from Table 2.2. In this section the DC motor is evaluated as the locomotion type for the transiently-powered robot.

#### Operation of a DC Motor

When voltage is applied to the motor, current rises as quickly as the inductance in the motor windings allows. DC motors produce an initial startup peak because the back electromotive force (back EMF) is initially zero. The current reaches a maximum when the rotor starts to rotate and a back EMF is generated. The back EMF increases further while the motor accelerates to its steady state speed, and the speed is determined by the voltage supplied.

If a load is applied to the DC motor, the current consumed by the motor is increased because current is proportional to the torque applied to the motor. Additionally, the angular velocity of the motor decreases while the torque is inversely proportional to the angular velocity of the motor.

#### Evaluation of the Start Current Peak

The DC motors used for robots are normally powered directly from the battery since linear or switch-mode power regulators are not able to supply the high start currents. However, the use of a supercapacitor requires a regulator to make efficient use of the energy stored, as described in Section 3.2.1. The switch-mode regulator that is part of the BQ25570 energy harvester is only able to supply a peak output current of 110 mA [28].

The 206-11 DC motor from Precision Microdrives [40] is the selected to be evaluated. From the datasheet a typical start current of 185 mA can be found for its rated operating voltage of 3 V. However, the system voltage chosen for transiently-powered robot is 2.2 V. To determine the startup current of a 206-110 motor when supplied with 2.2 V, a two second current trace is recorded using a Monsoon Power Monitor [41].

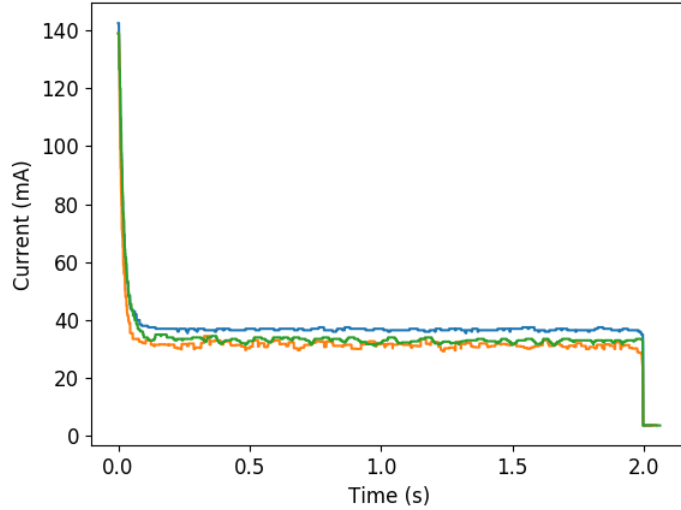


Figure 3.3: The free-running current profile of three 206-110 dc motors supplied with 2.2 V. Dc motors have a startup current peak significantly higher than their steady state current.

The maximum current measurements for three different motors is shown in Figure 3.3. The results show that a supply voltage of 2.2 V reduces the start current peak to 140 mA. This is still above 110 mA and the robot needs to power two motors in a differential drive configuration to allow steering.

A solution is to use Pulse Width Modulation (PWM) to reduce the motor speed and average current consumption. Combining PWM with a large bulk capacitor that can supply the short high current demand, should enable the buck converter to start the motors.

### 3.3.3 Conclusion

The only way the rotor and stator of a stepper motor aligned is by keeping the stepper motor coil energized. Frequent power interrupts could lead to loss of synchronization between the energized coil and position of the rotor as a result of rotor inertia. The error due to inertia becomes more significant with increase rotational speed. Loss of synchronization can result in random behavior of a differential drive robot, as one stepper motor may require a different amount of steps before synchronization than the other.

Normal DC motors have a high start current which the buck converter from the harvester might not be able to supply. PWM can be used to reduce the average current consumed by the motor and a large bulk capacitor can supply short high current demand from the motors. The DC motor is chosen as the locomotion type used for the transiently-powered robot.



## Chapter 4

# Design and Implementation

The hardware design of the transiently-powered robot is presented in Section 4.1. In Section 4.2 the controller is explained that allows the robot to perform controlled movements without external feedback. Finally, Section 4.3 introduces the software implementation that enables the robot to execute a movement despite regular power interrupts.

### 4.1 Hardware Design

The first step in the hardware design is to evaluate what components are required for the robot to have basic navigation capabilities. Commercially available low power components have been evaluated, where the main criteria was a low minimal supply voltage of 2.0 V to function with a system voltage of 2.2 V. In this section each part of the robot is explained in more detail. A complete overview of the robot is shown in Figure 4.1 and a complete assembled robot with WISP and solar panel is shown in Figure 4.2.

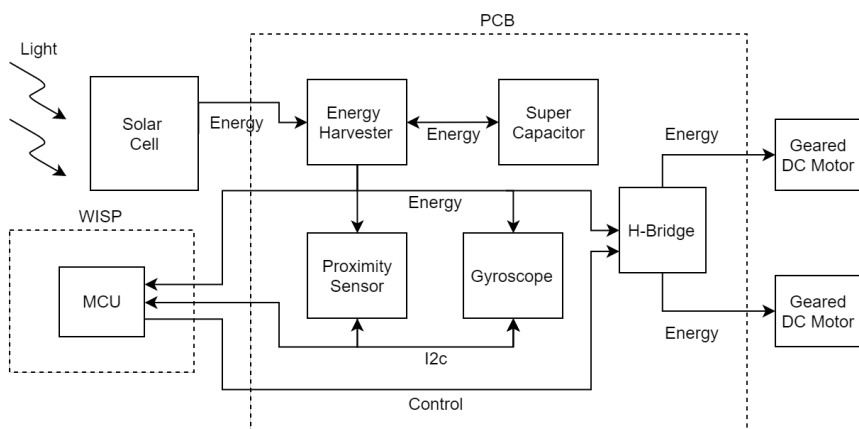


Figure 4.1: Schematic overview of the transiently-powered robot.

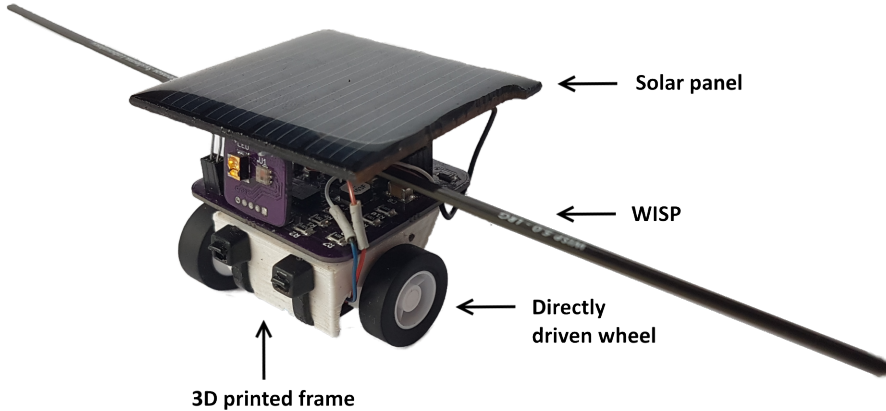


Figure 4.2: The complete robot with WISP and solar panel.

#### 4.1.1 Energy Harvesting and Storage

Energy is harvested from light using two IXYS SLMD121H04L-ND solar cells [35] in parallel, selected based on experimental results given in Section 3.2. The solar cells are connected to a Texas Instruments BQ25570 energy harvester [28] which stores the harvested energy in a 22 mF - 4.5 V supercapacitor from AVX [29].

#### 4.1.2 Computation

The robot is designed around a WISP5 [42], a battery-free platform for low power sensing, computation and communication. This platform has the ability to communicate with RFID readers and is powered by the carrier signal emitted by the reader. However, the communication range and the power that can be harvested is limited. Only the MCU from the WISP is currently being utilized: a Texas Instruments MSP430FR5969 ultra low power microcontroller. This MCU can operate at 16 MHz and features 64 KB FRAM, 2 KB SRAM and 40 IO-ports [43].

#### 4.1.3 Sensing

The robot has access to basic sensors which can be interfaced through I2C. For detecting obstacles in front of the robot, a Maxim Integrated MAX44000 proximity sensor [44] was added to the robot facing forward. The sensor switches an IR led at high frequency to reduce the power consumption. Because the sensor is based around a photo-diode it can be used to measure

the amount of ambient light as well. To allow for local motion feedback, the robot has a Bosch Sensortec BMG250 [45] low power triaxial gyroscope to measure yaw-rate.

#### 4.1.4 Locomotion

Sub-micro plastic planetary gearmotors from Precision Microdrives [40] are chosen to provide locomotion to the robot, as described in Section 3.3. Two motors are mounted diagonally opposite from each other in a 3D-printed frame making the robot as compact as possible, and the differential drive configuration allows steering. Small plastic wheels with rubber tires are mounted directly on each of the motor shafts. Behind the motors a free running caster wheel is mounted to the frame, acting as a third support point for the robot.

#### 4.1.5 Motor Control

The speed and the current consumption of each motor can be controlled individually using PWM. The MCU can use the H-bridge to enable, disable and control the direction of rotation of each individual motor. MCU output ports are limited in the amount of current that they can supply. MOSFETs inside a Texas Instruments DRV8836 dual H-bridge [46] allow efficient regulation of larger currents to the motors.

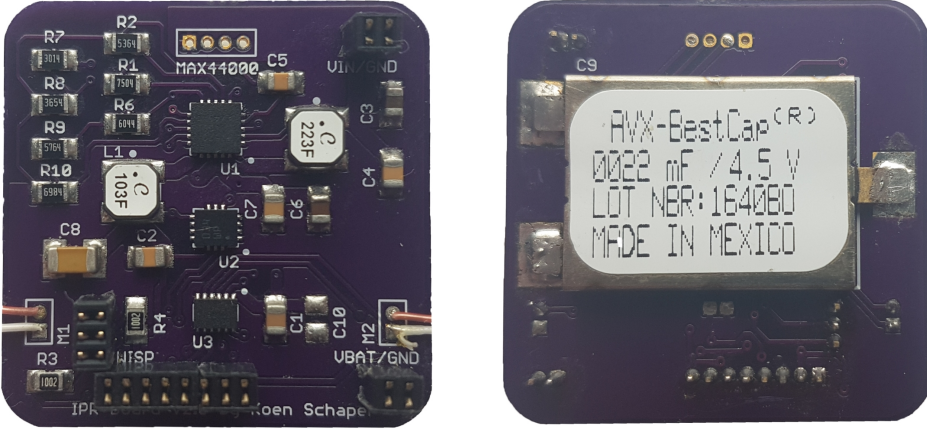
#### 4.1.6 Integration

Now that all the parts have been chosen, they can be connected together to form the robot. A Printed Circuit Board (PCB) has been designed using EAGLE PCB design and schematic software [47]. The PCB increases stability, eases connection and reduces of the total weight of the robot. Additionally, a PCB was required because of use of small size ICs (no lead packaging). A detailed schematic of the PCB can be found in Appendix A.

The size of the PCB is 30×30 mm, and an overview of both the top and bottom side of the PCB is shown in Figure 4.3. The PCB contains headers to connect the solar panel and headers to connect all the required pins from the WISP. An additional header is available to connect a battery for testing purposes. All the large components are mounted externally: the solar panel, WISP and the motors.

#### 4.1.7 Energy Expenditure

The average current consumption by each component is measured with a Monsoon Power Monitor [41]. The measurement is performed as follows: first a two second current trace was recorded of the current consumed by the MCU on the WISP. The MCU was then used to enable each component



(a) Top side of the PCB

(b) Bottom side of the PCB

Figure 4.3: The PCB designed for the robot, on the top side of the PCB the ICs are marked, harvester (U1), gyroscope (U2) and H-bridge (U3). The bottom side only contains the supercapacitor.

Table 4.1: Average consumed current for each individual component on the PCB at 2.2 V.

Part	Active Current
Proximity sensor	119 $\mu$ A
Gyroscope	848 $\mu$ A
Microcontroller @ 8MHz	522 $\mu$ A
H-bridge	349 $\mu$ A
Two DC motors <sup>1</sup>	27–50 mA
Total	29–52 mA

<sup>1</sup> Current consumed varies per motor and motor speed

individually, followed by a two second current measurement with the enabled component. The average of each current trace is calculated, and the current consumed by the microcontroller subtracted from the current consumed by each component. The measurements results are provided in Table 4.1.

#### 4.1.8 Costs

Using of off-the-shelf components that are readily available allows to build multiples of this robot with ease. Table 4.2 shows the total price per robot, assuming a minimal fabrication quantity of 20. This overview is compiled by querying the component prices of different suppliers, Farnell, Digikey, Mouser, Pololu, and OshPark. The price for the PCB does not include the

Table 4.2: Cost of parts for one robot

Part	Price (€)
Solar panel	9,60
Supercapacitor	7,43
Harvester	5,48
Proximity sensor	3,98
Gyroscope	2,81
H-bridge	1,47
Two DC motors	18,51
Wheels	3,08
PCB	2,50
Passive SMD	4,53
Total	59,39

price of assembling the PCB, as it is currently done by hand. Secondly, the cost of a WISP/MCU is currently not included in the price. From this table can be concluded that the cost of building a transiently-powered robot is comparable to the cost of other reference small robotic platforms, as seen in Table 2.2.

## 4.2 Motion Control Design

In order for the robot to make controlled movements, it needs to have a local heading feedback method. Since the buck converter supplies a constant voltage to the motors, voltage is eliminated as a factor in determining the motor speed. By making the assumption that the robot only travels on a flat surfaces, the steady state speed is considered “constant”.

### 4.2.1 PWM Frequency for Linear Motion Control

PWM is used to control the speed of the motors, as briefly addressed in Section 3.3.2. The maximum frequency that still allows linear speed control is dependent on the electrical characteristics of the motor. When the motor is at rest, its equivalent circuit consists of a resistance ( $R$ ) and inductance ( $L$ ) in series. If a voltage is applied to the motor, the rate at which the current rises is limited by the inductance. All RL circuits have a time constant:  $\tau = L/R$  and the current is considered to have reached its maximum steady state at  $5\tau$  [48]. The motors used for the robot have a typical resistance of  $R = 14.5 \Omega$  and an inductance of  $L = 70 \mu\text{H}$  [40]. Therefore, the minimum pulse width should be equal to

$$T_{\min} = 5 \frac{L}{R} = 24.14 \mu\text{s}. \quad (4.1)$$

Table 4.3: With the minimum duty cycle the robots just starts moving and the maximum duty cycle is determined by the power supply while it still can supply the motor start current.

	Robot 1	Robot 2	Robot 3
Min duty cycle left (%)	16	14	18
Min duty cycle right (%)	13	22	16
Max duty cycle (%)	30	36	34

If a minimum duty cycle  $D_{\min}$  of 5% is assumed, then the maximum PWM frequency becomes

$$f_{\max} = \frac{D_{\min}}{T_{\min}} \times 100 = 2071.25 \text{ Hz.} \quad (4.2)$$

The PWM frequency is set to 2 kHz and from Table 4.3 can be seen that the minimum duty cycle is always above 5%.

### Minimum Duty Cycle

The minimum duty cycle is determined by the torque that is required for the motors to be able to overcome the static friction between the wheels and a surface the robot is moving on. Each motor is physically different and the friction in the gearbox can variate as well, which results in different output speeds per motor. Since the robot uses two motors in differential drive configuration, a minimum duty cycle has to be found for each motor. This is accomplished by setting a duty cycle at which both motors are rotating and slowly backing it down until one or both motors stop turning, the minimum duty cycle for each motor can be seen in Table 4.3. The minimum duty cycle, allowing each wheel to rotate, is stored as a calibration value. If each motor is supplied their minimum duty cycle does not imply that the motors rotate at the same speed, i.e. that the robot makes a straight movement.

### Maximum Duty Cycle

The maximum duty cycle is bounded by the amount of current that the buck converter and bulk capacitor can supply, as shortly discussed in Section 3.3.2. Lowering the duty cycle reduces both the maximum current peak and the steady state current, which is used to reduce the motor start current demand. The maximum duty cycle can be found by increasing the minimum duty cycle of each motor with the same value until the robot is unable to start a movement. The last working value is stored as a calibration value to limit the duty cycle, and the average maximum duty cycle is given in Table 4.3. The maximum duty cycle values are all below the calculated free running maximum duty cycle, as previously determined in Section 3.3.2

Table 4.4: Ziegler-Nichols PID gain estimator chart [49].

$K_p$	$T_i$	$T_d$
$0.6K_u$	$T_u/2$	$T_u/8$

#### 4.2.2 Closed loop feedback for controlled movements

Open loop movement using calibrated motor values has been used in previous work [1], but it can be time consuming. Furthermore, any small disturbance can throw the robot off course. Controlled movements can be achieved by using closed loop feedback, where the heading is used to update the motor control values. The robots relative change in heading, i.e. horizontal angular velocity, can be obtained from the gyroscope and corresponds to the yaw-rate.

#### PID Controller

Closed loop feedback is achieved by use of a Proportional Integral Derivative (PID) controller. The input of the PID controller is the yaw-rate from the gyroscope. The controller periodically tries to reduce the yaw error as

$$e(t) = \psi_{\text{target}} - \psi(t), \quad (4.3)$$

where  $\psi_{\text{target}}$  is the yaw-rate target and  $\psi(t)$  the yaw-rate obtained by the gyroscope. The PID controller adjusts its output, and corrects the speed of each motor in opposite direction as

$$u(t) = K_p e(t) + K_i \int_0^t e(\tau) d\tau + K_d \frac{d}{dt} e(t), \quad (4.4)$$

where  $K_p$ ,  $K_i$  and  $K_d$  are the tunable gains from the PID controller. Using the gains, the controller is continuously adjusting the motor speed in order to reduce the error to zero.

#### Controlled movements

The robot is able to execute two distinct movement: straight and curved movements. When the robot executes a controlled straight movement, any movement perpendicular to the robots heading direction is undesired. The yaw-rate target is set to zero, forcing the PID controller to keep the robot straight. For curved movements however, a desired yaw-rate set point needs to be specified. The yaw-rate set point can for example be determined from the radius of the circle that the robot needs to turn and a calibrated speed.

### PID tuning using Ziegler-Nichols method

Tuning can be done by a trial and error approach, but a faster way of tuning is to use the closed loop Ziegler-Nichols method [49].

The method evaluates the amplitude and frequency of observed oscillations in the system by adjusting the tunable gains. Initially, the integral gain and the derivative gain,  $K_i$  and  $K_d$  respectively, are set to zero. Then, the proportional gain  $K_p$  is increased from zero until sustained oscillation occurs, which corresponds to the ultimate gain  $K_u$ . The ultimate period  $T_u$  is equal to the corresponding period and should be measured at zero crossings of the oscillation. The found ultimate gain and period can be used to determine the PID gains using Table 4.4.

### Experimental ultimate gain and period determination

To find the ultimate gain and period, a robot is programmed to execute a two second straight movement. The yaw-rate data is stored in non-volatile memory in order to retrieve it using a programmer, after the robot has performed the movement. In Figure 4.4a two second yaw-rate measurement traces are shown for several proportional gains. With a proportional gain of 0.13 the robot shows roughly constant oscillation. On the other hand, for a gain of 0.14 the robot shows unstable behavior due to a small disturbance after one second, resulting in oscillations that keep increasing in amplitude. The ultimate period is determined to be equal to  $T_u = 0.2$ , and is used together with the ultimate gain to determine the tuning parameters from the gain chart in Table 4.4. The integral gain and derivative gain can now be determined to be equal to  $K_i = K_p/T_u$  and  $K_d = K_p T_u$  respectively. Figure 4.4b shows how the oscillations are removed by setting the tunable gains according to the closed loop Ziegler-Nichols method. The tuning process was speeded up by setting the minimum motor duty cycle as it made the robot a lot more responsive, as described in Section 4.2.1.

## 4.3 Software Implementation

The software implementation that allows the robot to perform controlled movements is divided in three parts, the main program, a control loop and motor control. In the main program a set of movements can be defined for the robot to be executed. The robot can be controlled using three movement commands: (1) straight trajectories, (2) curved right turns and (3) curved left turns. For each movement an additional movement target needs to be defined that specifies the duration, i.e. when the control loop considers the movement to be finished.

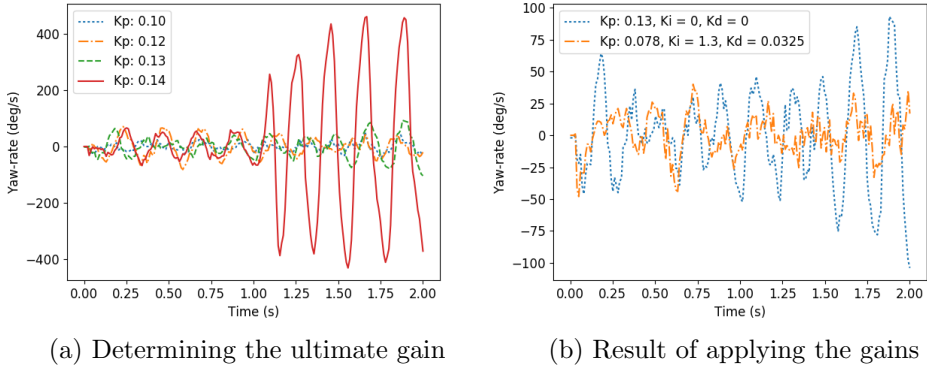


Figure 4.4: Tuning the PID controller using the closed loop Ziegler-Nichols method, first the ultimate gain is determined to be equal to 0.13. Then the ultimate period is determined equal to 0.2 and using Table 4.4 the tunable gains are determined.

### 4.3.1 Control loop

When the control loop receives a movement command, the yaw-rate set point, movement target and motor duty cycle target are set accordingly. A timer running at a frequency of a 100 Hz, is used to periodically call an interrupt service routine (ISR) and execute the control loop. Using an ISR has the benefit of a constant sample time, which simplifies the PID loop, because the integration and differentiation time are also constant and known in advance. When the ISR is triggered, first a yaw-rate sample is requested from the gyroscope, as seen in Figure 4.5. Based on the current movement command, an evaluation is performed to determine if the movement target is reached. If this is not the case, the yaw-rate is supplied to the PID controller, which in turn updates the motor values. The output value produced by the PID controller is subtracted from the left motor value and added to the right motor value, in order to keep the average speed approximately the same.

### Movement target

For straight movements the movement target is equal to a predetermined time, i.e. number of control loop timer trigger events. Curved movements use an angle movement target. By integrating the angular velocity an angle estimate is obtained, which is used to verify if the provided angle movement target is reached within a margin of two degrees. The loop exits automatically when the required movement target is reached.

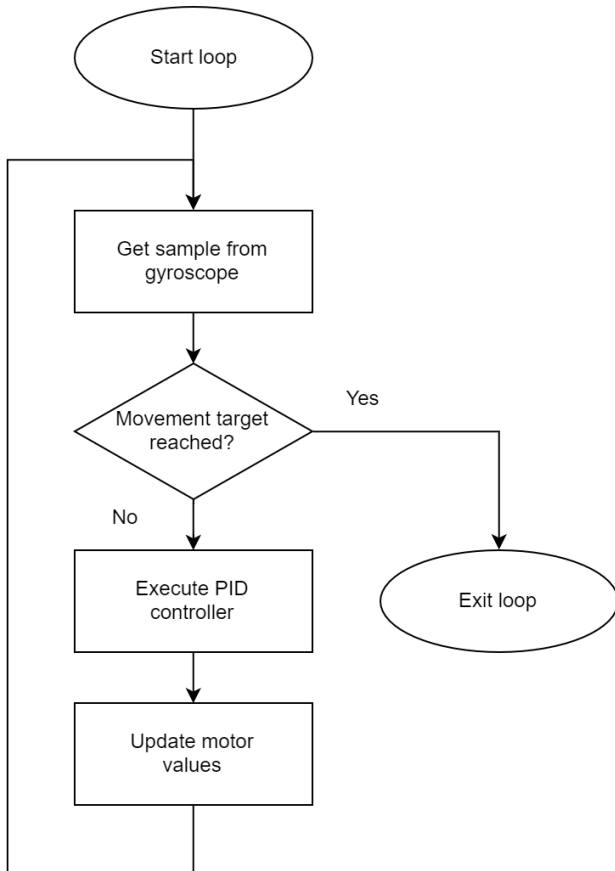


Figure 4.5: The control loop that periodically updates the motor values based on the yaw-rate obtained from the gyroscope. The loop exits automatically if the movement target is reached.

#### 4.3.2 Motor Control

The motors are controlled using PWM signals generated by a second timer, which runs at the predetermined frequency of 2 kHz. The timer is able to directly control the four IO-ports connected to the H-bridge, eliminating the overhead of an ISR. The H-bridge is configured such that two IO-ports directly control a motor. If one of the ports is enabled the motor rotates forwards and if the other port is enabled the motor rotate backwards. The control loop updates the compare registers corresponding to each of the ports. The minimum duty cycle value is added to each motor value and is bounded by the maximum duty cycle. When the timer reaches a value that corresponds to the value stored in one of the compare registers, the connected port is toggled automatically.

### **4.3.3 Persistent Movement**

The transiently-powered robot can make one movement or a series of movements, which probably requires multiple power cycles to complete. To be able to finish a movement and not reset, i.e. redo the same movement, a simple checkpointing method is used to save the progress across power cycles. A persistent counter registers the progress in the set of movements. Every control loop iteration the persistent variable that captures the progress towards the movement target is updated, and depending on the movement can be a time or angle. The right and left motor speed tuned by the PID controller are not saved and restored after a power interrupt. Due to the startup phase of the motors, previously tuned motor speeds are suspected to be invalid and cannot be used after a power interrupt.

### **4.3.4 Extendability**

The current software implementation consists of 700 lines of MSP430 specific C code, that takes up 14% of the SRAM and 14% of the FRAM. The control loop is implemented using an ISR leaving the main processor available for other computation tasks. The backscatter communication channel on the WISP is currently not implemented, but can potentially be used to provide communication with a global host. Two of the five available timers are used for the control loop and the motor control, while the other three timers are used by the WISP software communication stack.



# Chapter 5

## Evaluation

### 5.1 Controlled Movements

In this section the accuracy of movement of the battery-less robot is evaluated and compared to its battery powered counterpart.

#### 5.1.1 Experimental setup

To be able to compare the accuracy of the robot while it is exposed to increasingly smaller on times, a variety of movements is recorded using an overhead camera. A stand with a Nikon D610 DSLR camera is positioned on a tabletop, as seen in Figure 5.1a. The corners of a square of  $80 \times 80$  cm are indicated with black corner markers. This square is used as a reference to convert the robots movement from pixels to cm. Two movements are compared: (1) the robot performs a straight movement of 75 cm and (2) the robot performs a circular movement of 360 degrees with a radius of 30 cm.

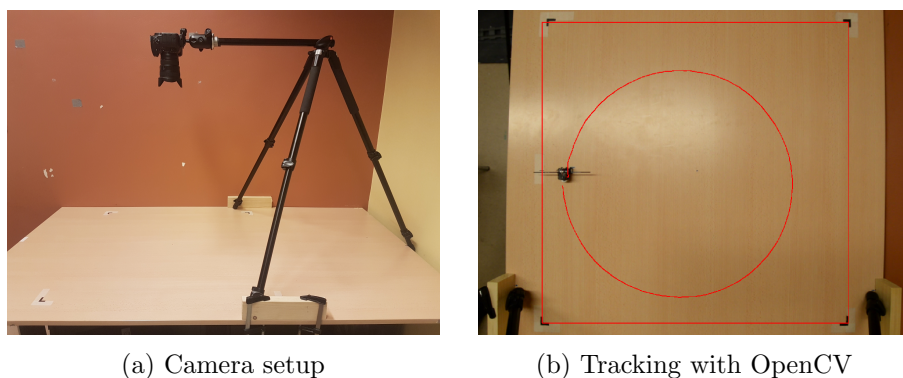


Figure 5.1: Experimental setup to record the robots movement.

## Tracking the Movement

Before the robot executes the movement, a green marker is placed on top of the robot. The marker is the reference point that is used by the tracking software. The camera is used to record the movement, which then is analyzed using Python and OpenCV 3.2. An example of a tracked movement can be seen in Figure 5.1b. The red square is drawn using OpenCV and visually sized to fit the square marked by the black corner markings on the table top. Because the size of the square is known to be  $80 \times 80$  cm, the movement coordinates can be converted from pixels to centimeter.

## Target Duty Cycle

To evaluate the influence of speed on the movement accuracy, each movement is executed at three different target duty cycle settings: 40%, 65% and 90% of the maximum duty cycle. The maximum duty cycle is previously determined in Section 4.2.1, by the amount of current that the power supply can deliver to the motors. The highest setting is chosen to be equal to 90% because it allows the PID controller to also increase the target duty cycle. If the target duty cycle is set to a 100 %, the controller is only able to decrease the speed of the faster rotating motor because the maximum motor speed is bounded at a 100 %.

## Power Interrupts

The on time is determined by the energy stored in the capacitor and the power consumed by the robot for movement. To evaluate different on times, besides the one created with the 22 mF supercapacitor, additional power interrupts are generated artificially. The power interrupts, i.e. the capacitor running out of energy, are created artificially using a timer that resets the MCU. If the interrupts are generated artificially, the robot is powered from a battery. The MSP430FR5969 has the functionality to enable a brownout reset through software, which is used to simulate the event of the supply voltage dropping below the required operating voltage [50]. A timer is used to generate the power interrupt after a predefined on time.

## On Time

With the selected capacitor of 22 mF, the robot can operate around 1 second. To find the minimal on time that is required to allow control of the robot, it is programmed to perform a four second straight movement. The movement is recorded for each target duty cycle and the on times of 0.4 s, 0.3 s and 0.2 s are evaluated.

The results in Figure 5.2 show that for the higher duty cycle targets an on time of 0.3 s leads to significant drift to one side, which is classified

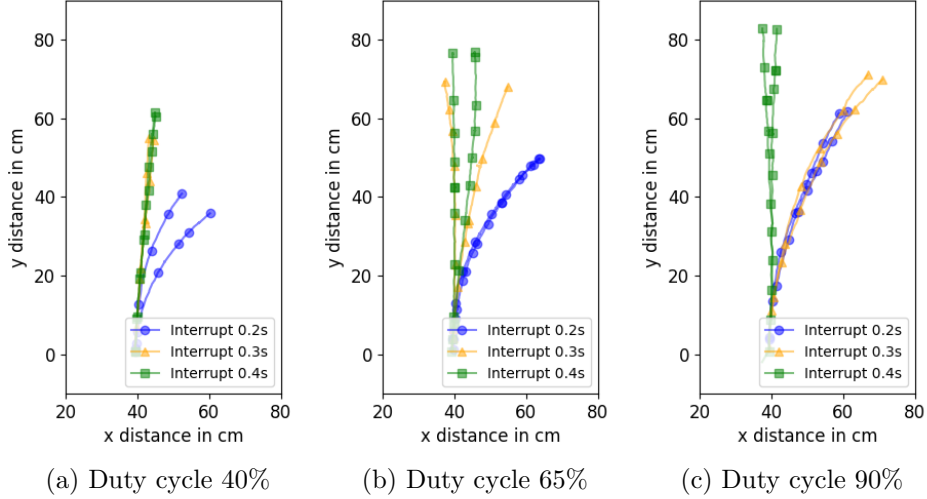


Figure 5.2: Accuracy of four second straight movements while the on time is decreased, for each target duty cycle.

as uncontrolled behavior. The control loop was not able to stabilize the movement before a power interrupt occurs, and therefore the robot drifts to the side of its weakest motor. The duration that power is available might not be long enough for the motors to reach their steady state speed, making linear control of the motors impossible. Increasing the target duty cycle shows that a longer on time is required to control the movement. Therefore, the on times evaluated in this experiment are set to 1.0 s and 0.5 s.

### Speed Calibration

Another observation stemming from the results in Figure 5.2, is the distance covered by the robot decreases by decreasing the target and/or on time. Without any sensors or external feedback of the robots speed, it is difficult to determine the distance that the robot has traveled. A rough speed estimate allows the robot calculate the traveled distance and stay within the view of the camera. The average speed is estimated for each target duty cycle and one time combination. This is achieved by first determining the time that the robot requires to move approximately 150 cm for each target duty cycle without power interrupts. When the robot experiences power interrupts, the average speed of an active period becomes lower due to frequent acceleration from a standstill. Therefore, power interrupts increase the runtime required to make the robot travel approximately the same distance.

Finally, the average of five complete movement measurements is computed and divided by the commanded runtime of the robot to acquire an average

Table 5.1: The calibrated speeds in centimeter per second for each target duty cycle and on time combination.

Duty cycle (%)	No interrupt	1.0 s	0.5 s	Solar
40	18.9	18.0	15.9	16.0
65	24.0	21.3	18.8	20.8
90	28.8	25.7	22.7	23.3

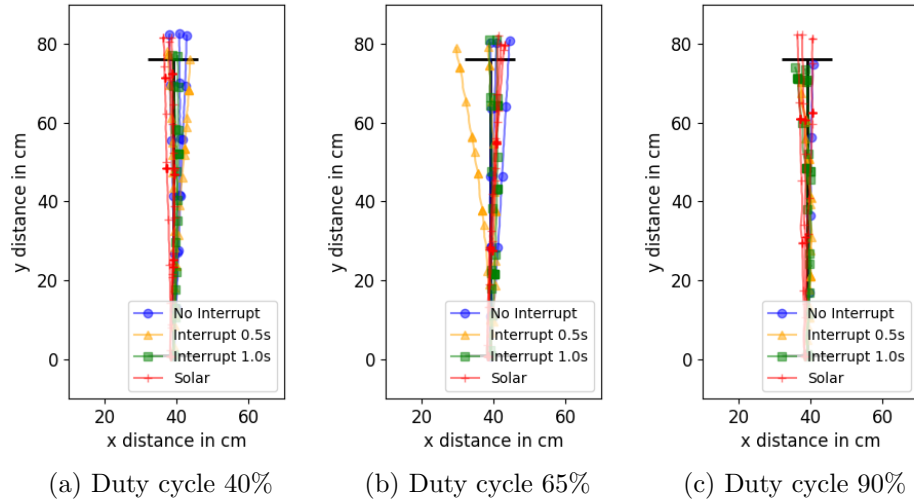


Figure 5.3: Straight movements for the different target duty cycles, the black horizontal line marks the 75 cm endpoint.

speed for each combination, as seen from Table 5.1.

### 5.1.2 Straight Movements

Using the calibrated speeds and selected on times, the robot is commanded to perform a straight movement of 75 cm from position (40,0) cm within the reference frame. Each combination is recorded multiple times and the motion data is extracted from the video using Python and OpenCV. The results in Figure 5.3 show that the distance traveled by the robot, for each measurement, approximates the commanded 75 cm. Additionally, the results show a varying horizontal deviation between the start and end point. The horizontal deviation may be a consequence of inaccuracy in performing the movement. However, it is more likely that the error originates from in the start position of the robot, because the robot is expected to not be positioned exactly perpendicular to the reference frame of 80×80 cm. Even though the robot is positioned carefully in the same start position, it is inevitable the start angle is not exactly equal to other measurements.

Table 5.2: The Euclidean distance between the measurements and a reference line computed between start and end coordinates.

Duty cycle (%)	Interrupt (s)	Max (cm)	Mean (cm)	Std (cm)
40	No interrupt	0.86	0.36	0.16
	1.00	1.35	0.56	0.27
	0.50	0.86	0.44	0.22
	Solar	0.50	0.25	1.35
65	No interrupt	0.52	0.25	0.12
	1.00	0.91	0.44	0.21
	0.50	2.15	1.17	0.54
	Solar	0.41	0.17	1.05
90	No interrupt	0.54	0.28	0.13
	1.00	1.76	0.95	0.42
	0.50	2.18	1.09	0.61
	Solar	0.30	0.15	0.69

### Movement Accuracy Metrics

The robot has no reference to its surroundings to determine its absolute position and heading direction, i.e. no external feedback. Therefore, only relative metrics are assumed to be valid. For each measurement a reference line is computed between the first and last measured data point. The Euclidean distance between the closest measurement and the reference line is computed.

### Straight Movement Results

The results for the battery powered robot with and without artificial interrupts show that decreasing the on time, increases the maximum, average and standard deviation of the horizontal deviation, as seen in Table 5.2. Increasing the speed does not have the same effect and no significant differences can be seen from the results.

The solar powered shows less horizontal deviation when compared to the battery powered robot. This seems counter-intuitive, but there is a suspicion that the additional weight of the solar panel has a big effect on the movement of the robot. The weight of the solar panel is more than twice that of the battery, 5.2 g and 2.1 g respectively, and is more evenly distributed over the robot. The robot without a battery or solar panel has a weight of 16.7 g and therefore the weight of the solar panel can be considered significant when compared to the bare weight of the robot.

### 5.1.3 Circular Movements

The robot is programmed to make a circle with radius of 30 cm with the predetermined speed and on times. The results in Figure 5.4 show that for all measurements the robot is able perform the circular movement. A clear difference in circle radius can be seen for each on time, as a result of an error between the actual and calibrated speeds. The robot sometimes overshoots its final position. It is expected to be caused by an error in integration of the angular velocity to obtain an angle. The angle is used to determine if the movement target is reached. Decreasing the power interrupt frequency is suspected to increases the integration error due to frequent accelerations from zero by the robot.

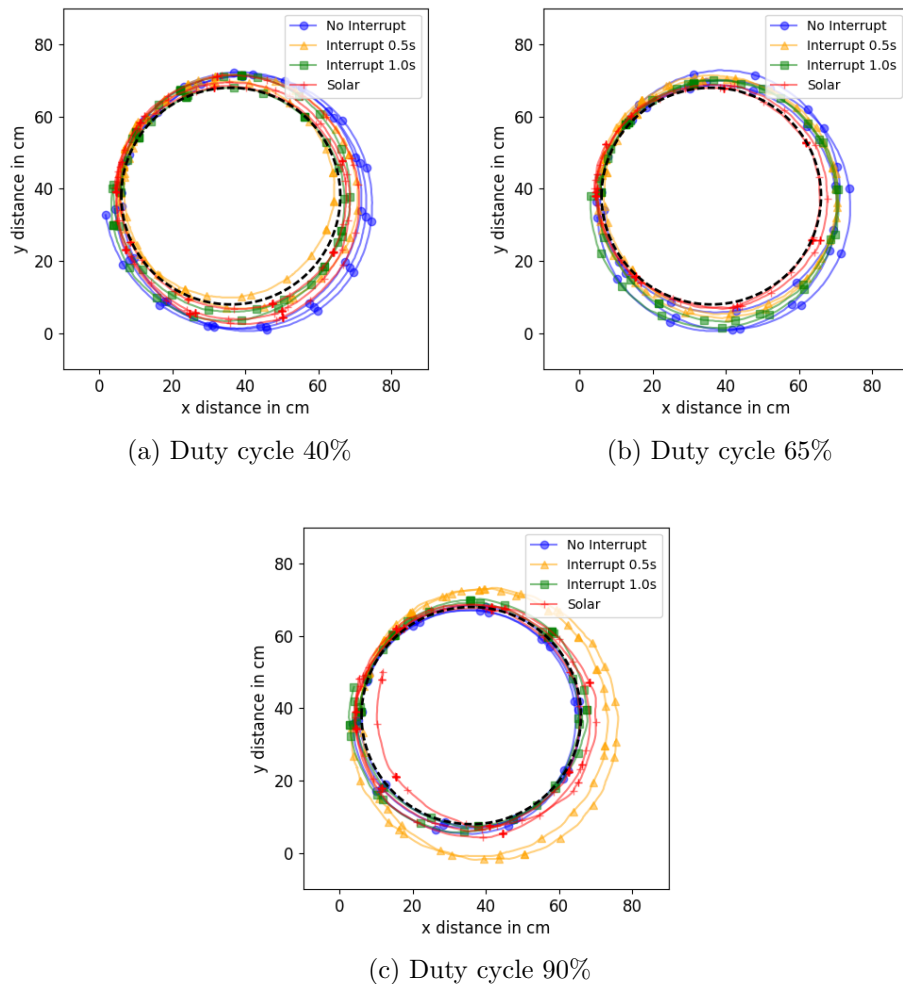


Figure 5.4: Circular movements for the different target duty cycles, the black dashed circle marks the programmed circle with a radius of 30 cm.

Table 5.3: The Euclidean distance between the measurements and a best fitting circle.

Duty cycle (%)	Interrupt (s)	Radius (cm)	Max (cm)	Mean (cm)	Std (cm)
40	No interrupt	34	4.30	1.30	0.67
	1.00	32	3.95	1.52	0.81
	0.50	32	6.08	1.85	1.30
	Solar	32	1.93	0.89	0.46
65	No interrupt	34	3.03	1.2	0.67
	1.00	32	4.20	1.42	0.92
	0.50	32	1.86	0.79	0.34
	Solar	31	1.93	0.88	0.4
90	No interrupt	30	2.37	0.9	0.45
	1.00	31	3.50	1.06	0.65
	0.50	35	4.53	1.69	1.23
	Solar	31	2.10	0.88	0.37

### Movement Accuracy Metrics

To determine the accuracy of the circular movement, a circle with varying radius is visually fitted to data of each movement. The radius is different because calibrated speed varies with each target duty cycle and on time. The Euclidean distance is computed between the reference circle and the measured circular movements.

### Circular Movement Results

The average deviation from the reference circle reduces when the target duty cycle is increased, as seen from Table 5.3. The additional speed is likely to provide more stability to the movement, since less interrupts are experienced while the circular movement is completed, i.e. the controller is able to provide more direction. The solar powered robot shows more stability when compared to the battery powered robot. Which is expected to be a positive effect of the additional solar panel weight, as explained in the results of Section 5.1.2.



# Chapter 6

## Summary

This thesis is surmised by a conclusion in Section 6.1 and in Section 6.2 possibilities for future work are presented.

### 6.1 Conclusion

In this thesis, a transiently-powered battery-free robot is designed and implemented. The robot harvests energy from light and DC motors are chosen to provide locomotion. An embedded gyroscope provides heading feedback, and a PID controller allows execution of controlled straight and curved movements. A simple check pointing method combined with persistent movement targets allows a movement to be completed across multiple power cycles.

Straight and circular movements are executed and recorded using an overhead camera. Tracking software is used to collect the robots movement data and compare the movement accuracy of a transiently-powered battery-free robot with its battery powered equivalent. Using artificial power interrupts, the on time is decreased and a lower threshold of 0.3s is found. The robot started to show uncontrolled behavior, i.e. significant drift to the side of the weakest motor. On times below 0.3s might not allow the motors to reach their steady state speed, making linear motor control impossible.

The results show that decreasing the on time towards the lower threshold, increases the horizontal deviation in case of straight movements. It is expected to be caused by more frequent accelerations from standstill. For curved movements the results show a decreased average deviation from the fitted circle by increasing the target duty cycle. The additional speed is suspected to allow the controller to be more effective in steering the robot towards its final destination. The solar powered robot surprisingly outperforms the battery-powered robot in terms of movement accuracy. The additional weight of the solar panel is likely to have a positive effect on the movement of the robot.

## 6.2 Future Work

The capabilities of the current robot can easily be extended by using more features from the WISP or by designing a custom alternative. Additional features that could be implemented in future work are:

- **Speed feedback:** In order to move a certain distance with a higher accuracy, an energy efficient speed feedback method is required. One option is to add local speed sensing or another option is to supply external position feedback to the robot.
- **Communication:** Communication with an external host is not implemented. The backscatter communication channel of the WISP could be used.
- **Transiently-powered swarm:** With an implemented communication channel, a promising new area of research is transiently-powered swarms. The effect of intermittency on the behavior and controllability of this type of swarm needs further investigation. The applicability of existing swarm algorithms is currently unknown and new methods might be required.
- **Size reduction:** In order to further reduce the weight of a robot, an alternative to DC motors has to be found. Unfortunately, significant smaller and efficient DC motors are not available. Miniature legged robots that make use of piezoelectric actuators seem promising, but most of them are still in an early stage of development.
- **Sensing capabilities:** Future applications may require additional sensors to be added to the robot to extend its capabilities. However, the power consumption, frequency of use and the accuracy trade off needs to be evaluated carefully since the energy budget is limited.

# Bibliography

- [1] M. Le Goc, L. H. Kim, A. Parsaei, J.-D. Fekete, P. Dragicevic, and S. Follmer, “Zooids: Building blocks for swarm user interfaces,” in *Proc. ACM UIST*, Tokyo, Japan, Oct. 16–19, 2016, pp. 97–109.
- [2] A. Dementyev, H.-L. C. Kao, I. Choi, D. Ajilo, M. Xu, J. A. Paradiso, C. Schmandt, and S. Follmer, “Rovables: Miniature on-body robots as mobile wearables,” in *Proc. ACM UIST*, Tokyo, Japan, Oct. 16–19, 2016, pp. 111–120.
- [3] (2017) Sony adds toio cubes to its arsenal of strange robotic toys. [Online]. Available: <https://spectrum.ieee.org/automaton/robotics/home-robots/sony-adds-toio-cubes-to-its-arsenal-of-strange-robotic-toys>
- [4] J. C. Barca and Y. A. Sekercioglu, “Swarm robotics reviewed,” *Robotica*, vol. 31, no. 3, pp. 345–359, May 2013.
- [5] S. N. Patel and J. R. Smith, “Powering pervasive computing systems,” *IEEE Pervasive Comput.*, vol. 16, no. 3, pp. 32–38, Jul. 2017.
- [6] G. P. Zachary, “The search for a better battery: Government funding and venture capital won’t buy us better batteries anytime soon [Spectral Lines],” *IEEE Spectrum*, vol. 53, no. 5, pp. 7–7, Apr. 2016.
- [7] C. Konstantopoulos, E. Koutroulis, N. Mitianoudis, and A. Bletsas, “Converting a plant to a battery and wireless sensor with scatter radio and ultra-low cost,” *IEEE Trans. Instrum. Meas.*, vol. 65, no. 2, pp. 388–398, Feb. 2016.
- [8] A. P. Sample, D. J. Yeager, P. S. Powledge, A. V. Mamishev, and J. R. Smith, “Design of an rfid-based battery-free programmable sensing platform,” *IEEE Trans. Instrum. Meas.*, vol. 57, no. 11, pp. 2608–2615, Nov. 2008.
- [9] J. Gummeson, S. S. Clark, K. Fu, and D. Ganesan, “On the limits of effective hybrid micro-energy harvesting on mobile CRFID sensors,” in

*Proc. ACM MobiSys*, San Francisco, CA, USA, Jun. 15–18, 2010, pp. 195–208.

- [10] S. Naderiparizi, A. N. Parks, Z. Kapetanovic, B. Ransford, and J. R. Smith, “Wispcam: A battery-free rfid camera,” in *Proc. IEEE RFID*, San Diego, CA, USA, Apr. 15–17, 2015, pp. 166–173.
- [11] B. Ransford, J. Sorber, and K. Fu, “Mementos: System support for long-running computation on rfid-scale devices,” in *Proc. ACM AS-PLoS*, New York, NY, USA, Mar. 5–11, 2011, pp. 159–170.
- [12] J. Van Der Woude and M. Hicks, “Intermittent computation without hardware support or programmer intervention,” in *Proc. OSDI*, Berkeley, CA, USA, Nov. 2–4, 2016, pp. 17–32.
- [13] A. Colin and B. Lucia, “Chain: Tasks and channels for reliable intermittent programs,” in *Proc. ACM OOPSLA*, Amsterdam, Netherlands, Nov. 30–4, 2016, pp. 514–530.
- [14] R. V. Prasad, S. Devasenapathy, V. S. Rao, and J. Vazifehdan, “Reincarnation in the ambiance: Devices and networks with energy harvesting,” *IEEE Commun. Surveys Tuts.*, vol. 11, no. 1, pp. 195–213, First Quarter 2014.
- [15] Maxwell Technologies, Inc. (2017) Ultracapacitor overview flyer. [Online]. Available: [http://www.maxwell.com/images/documents/Ultracapacitors\\_Overview\\_Flyer\\_3000615-2EN.pdf](http://www.maxwell.com/images/documents/Ultracapacitors_Overview_Flyer_3000615-2EN.pdf)
- [16] The Guardian. (2017) Samsung blames two separate battery faults for galaxy note 7 fires. [Online]. Available: <https://www.theguardian.com/technology/2017/jan/23/samsung-blames-faulty-batteries-for-causing-galaxy-note-7-fires>
- [17] A. Gonzlez, E. Goikolea, J. A. Barrena, and R. Mysyk, “Review on supercapacitors: Technologies and materials,” *Renewable and Sustainable Energy Reviews*, vol. 58, no. Supplement C, pp. 1189–1206, May 2016.
- [18] M. Rubenstein, B. Cimino, R. Nagpal, and J. Werfel, “Aerobot: An affordable one-robot-per-student system for early robotics education,” in *Proc. IEEE ICRA*, Seattle, WA, USA, May 26–30, 2015, pp. 6107–6113.
- [19] A. P. Sabelhaus, D. Mirsky, L. M. Hill, N. C. Martins, and S. Berbreiter, “TinyTeRP: A tiny terrestrial robotic platform with modular sensing,” in *Proc. IEEE ICRA*, Karlsruhe, Germany, May 6–10, 2013, pp. 2600–2605.

- [20] D. Pickem, M. Lee, and M. Egerstedt, “The GRITSBot in its natural habitat - a multi-robot testbed,” in *Proc. IEEE ICRA*, Seattle, WA, USA, May 26–30, 2015, pp. 4062–4067.
- [21] J. Y. Kim, T. Colaco, Z. Kashino, G. Nejat, and B. Benhabib, “mROBerTO: A modular millirobot for swarm-behavior studies,” in *Proc. IEEE/RSJ IROS*, Daejeon, Korea, Oct. 9–14, 2016, pp. 2109–2114.
- [22] M. Rubenstein, C. Ahler, and R. Nagpal, “Kilobot: A low cost scalable robot system for collective behaviors,” in *Proc. IEEE ICRA*, Saint Paul, MN, USA, May 14–18, 2012, pp. 3293–3298.
- [23] A. T. Baisch and R. J. Wood, “Pop-up assembly of a quadrupedal ambulatory microrobot,” in *Proc. IEEE/RSJ IROS*, Tokyo, Japan, Nov. 3–7, 2013, pp. 1518–1524.
- [24] N. K. Ure, G. Chowdhary, T. Toksoz, J. P. How, M. A. Vavrina, and J. Vian, “An automated battery management system to enable persistent missions with multiple aerial vehicles,” *IEEE/ASME Trans. Mechatronics*, vol. 20, no. 1, pp. 275–286, Feb. 2015.
- [25] J. Zhang, G. Song, Y. Li, G. Qiao, and Z. Li, “Battery swapping and wireless charging for a home robot system with remote human assistance,” *IEEE Trans. Consum. Electron.*, vol. 59, no. 4, pp. 747–755, Nov. 2013.
- [26] M. Karpelson, B. H. Waters, B. Goldberg, B. Mahoney, O. Ozcan, A. Baisch, P.-M. Meyitang, J. R. Smith, and R. J. Wood, “A wirelessly powered, biologically inspired ambulatory microrobot,” in *Proc. IEEE ICRA*, Hong Kong, China, May 31 – Nov. 4 2014, pp. 2384–2391.
- [27] R. Brhwiler, B. Goldberg, N. Doshi, O. Ozcan, N. Jafferis, M. Karpelson, and R. J. Wood, “Feedback control of a legged microrobot with on-board sensing,” in *Proc. IEEE/RSJ IROS*, Hamburg, Germany, Sept 28 – Oct. 2 2015, pp. 5727–5733.
- [28] Texas Instruments. (2017) Bq25570 ultra low power harvester power management ic with boost charger, and nanopower buck converter. [Online]. Available: <http://www.ti.com/product/bq25570>
- [29] AVX. (2017) Bestcap bz series. [Online]. Available: <http://www.avx.com/products/supercapacitors/bestcapreg-bz-series/>
- [30] Saleae. (2017) Logic analyser. [Online]. Available: <https://www.saleae.com/>

- [31] Impinj. (2017) Impinj end-of-life (eol) products. [Online]. Available: <https://support.impinj.com/hc/en-us/articles/217295087-Impinj-End-of-Life-EOL-Products>
- [32] ——. (2017) Indy r1000 datasheet. [Online]. Available: <https://support.impinj.com/hc/en-us/articles/202755848-Indy-R1000-Datasheet>
- [33] Laird Technology. (2017) S9028pcr rfid panel antenna. [Online]. Available: <https://www.lairdtech.com/products/s9028pcr>
- [34] (2017) Banggood polycrystalline solar panel. [Online]. Available: [https://www.banggood.com/2V-0\\_14W-70MA-40-x-40-x-3\\_0mm-Polycrystalline-Silicon-Solar-Panels-Epoxy-p-1013199.html](https://www.banggood.com/2V-0_14W-70MA-40-x-40-x-3_0mm-Polycrystalline-Silicon-Solar-Panels-Epoxy-p-1013199.html)
- [35] IXOLAR. (2017) High efficiency solarmd slmd121h04l. [Online]. Available: [http://ixapps.ixys.com/datasheet/slmd121h04l\\_nov16.pdf](http://ixapps.ixys.com/datasheet/slmd121h04l_nov16.pdf)
- [36] Azurspace. (2017) Space solar cells. [Online]. Available: <http://www.azurspace.com/index.php/en/products/products-space/space-solar-cells>
- [37] G. Grandi, A. Ienina, and M. Bardhi, “Effective low-cost hybrid led-halogen solar simulator,” *IEEE Transactions on Industry Applications*, vol. 50, no. 5, pp. 3055–3064, Sep. 2014.
- [38] Philips. (2017) Infrared industrial heat incandescent. [Online]. Available: <http://www.lighting.philips.com/main/prof/conventional-lamps-and-tubes/special-lamps/infrared/infrared-industrial-heat-incandescent>
- [39] Nidec Sankyo Corporation. (2017) Pm type stepping motors ms1t series. [Online]. Available: <http://www.nidec-sankyo.co.jp/english/product/motor/data/ms1t.pdf>
- [40] Precision Microdrives. (2017) 6mm dc gearmotor - 16mm type - model:206-110. [Online]. Available: <https://www.precisionmicrodrives.com/product/206-110-6mm-dc-gearmotor-16mm-type>
- [41] Monsoon Solutions, Inc. (2017) Powermonitor. [Online]. Available: <https://www.msoon.com/LabEquipment/PowerMonitor/>
- [42] (2017) Wisp 5.0 wiki. [Online]. Available: <http://wisp5.wikispaces.com/>
- [43] Texas Instruments. (2017) Msp430fr5969 16 mhz ultra-low-power microcontroller featuring 64 kb fram, 2 kb sram, 40 io. [Online]. Available: <http://www.ti.com/product/msp430fr5969>

- [44] Maxim Integrated. (2017) Max44000 ambient and infrared proximity sensor. [Online]. Available: <https://www.maximintegrated.com/en/products/analog/sensors-and-sensor-interface/MAX44000.html>
- [45] Bosch Sensortec. (2017) Bmg250 gyroscopes. [Online]. Available: [https://www.bosch-sensortec.com/bst/products/all\\_products/bmg250](https://www.bosch-sensortec.com/bst/products/all_products/bmg250)
- [46] Texas Instruments. (2017) Drv8836 1.5a low voltage stepper or single/dual brushed dc motor driver (pwm or ph/en ctrl). [Online]. Available: <http://www.ti.com/product/drv8836>
- [47] Autodesk. (2017) Eagle, pcb design made easy. [Online]. Available: <https://www.autodesk.com/products/eagle/overview>
- [48] Precision Microdrives. (2017) Pwm frequency for linear motion control. [Online]. Available: <https://www.precisionmicrodrives.com/application-notes/ab-022-pwm-frequency-for-linear-motion-control>
- [49] G. F. Franklin, J. Powell, and A. Emami-Naeini, *Feedback Control of Dynamic Systems, Global Edition*. Pearson Education Limited, 2015. [Online]. Available: <https://books.google.nl/books?id=ZV-pBwAAQBAJ>
- [50] Texas Instruments. (2017) Msp430fr58xx, msp430fr59xx, and msp430fr6xx family user's guide (rev. n). [Online]. Available: <http://www.ti.com/lit/ug/slau367n/slau367n.pdf>



## Appendix A

# Schematic of the Robot PCB

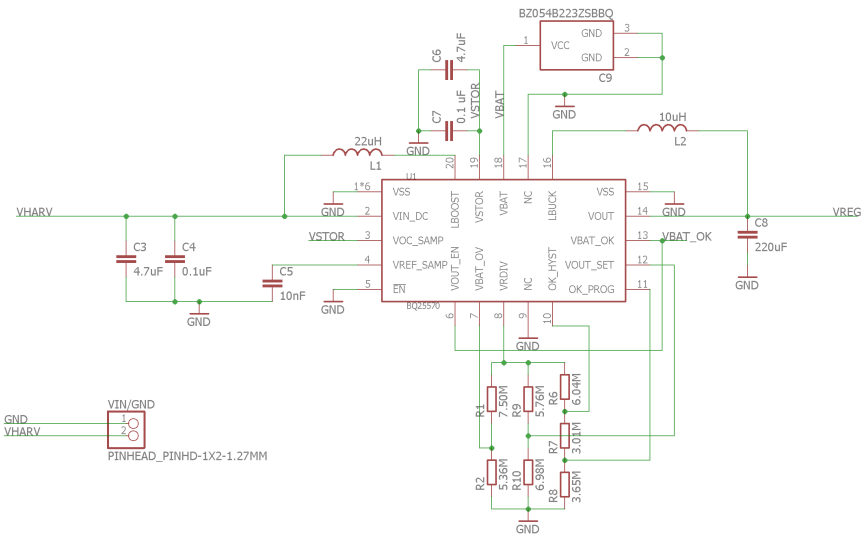


Figure A.1: Energy harvester part of the schematic

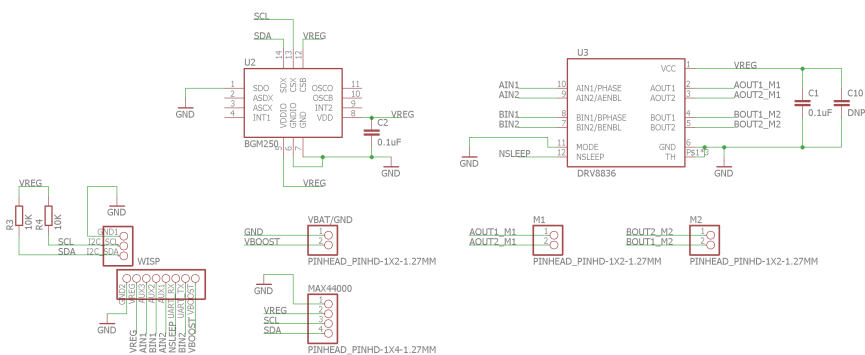


Figure A.2: Sensing and control part of the schematic